Citation: BoneKEy Reports **5**, Article number: 842 (2016) | doi:10.1038/bonekey.2016.75

www.nature.com/bonekey

LABORATORY METHODS

Tissue-engineered 3D cancer-in-bone modeling: silk and PUR protocols

Ushashi Dadwal[1,7], Carolyne Falank[2,7], Heather Fairfield[2,7], Sarah Linehan[2], Clifford J Rosen[2,3], David L Kaplan[4], Julie Sterling[5,6] and Michaela R Reagan[2,3]

[1]Department of Chemical and Biomolecular Engineering, Vanderbilt University, Nashville, TN, USA. [2]Maine Medical Center Research Institute, Scarborough, ME, USA. [3]Tufts University School of Medicine, Boston, MA, USA. [4]Department of Biomedical Engineering, Tufts University, Medford, MA, USA. [5]Center for Bone Biology, Division of Clinical Pharmacology, Vanderbilt University Medical Center, Nashville, TN, USA. [6]Department of Veterans Affairs, Tennessee Valley Healthcare System, Nashville, TN, USA.

Cancers that metastasize or grow in the bone marrow are typically considered incurable and cause extensive damage to the bone and bone marrow. The bone is a complex, dynamic, three-dimensional (3D) environment composed of a plethora of cells that may contribute to, or constrain, the growth of tumor cells and development of bone disease. The development of safe and effective drugs is currently hampered by pre-clinical two-dimensional (2D) models whose poor predictive power does not accurately predict the success or failure of therapeutics. These inadequate models often result in drugs proceeding through extensive pre-clinical studies only to fail clinically. Consistently, 3D co-culture systems prove superior to 2D mono-cultures in modeling *in vivo* cell phenotypes, disease progression and response to therapeutics. As a complex, multicellular, multidimensional bone microenvironment, 3D models allow for more accurate predictions of tumor growth, cell–cell and cell–matrix interactions, and resulting therapeutic responses. In this review we will discuss various 3D models available and describe step-by-step protocols for two of the most well-established 3D culture models for studying tumor-induced bone disease.

BoneKEy Reports **5**, Article number: 842 (2016) | doi:10.1038/bonekey.2016.75

Introduction

Despite decades of research in pathologies caused by bone metastatic tumors (breast, prostate, renal and lung), multiple myeloma (MM) and primary bony invasive tumors (osteosarcoma, oral cancer and melanoma), tumor-induced bone disease continues to be a clinical problem that causes pain and increased fracture risk in patients.[1] The lack of models that accurately mimic the complexity of the bone, whereas allowing for detailed molecular analysis, has been a major obstacle for progress. Thus, many groups have developed 3D models to enable longitudinal investigation of fundamental cell–cell and cell–matrix interactions in the complex cancer microenvironment over time.

Biomimetic 3D tissue-engineered systems have been developed for numerous diseases, but the complexity of bone has caused a lag in the development of appropriate 3D bone models. When developing 3D models of bone and cancer, many parameters are important including the strength, pore size, mineral composition and fluid flow, which are significantly different in the bone than any other tissue in the body. It is critical to accurately mimic these conditions as it has been demonstrated that matrix rigidity influences cancer invasion, metastasis and tissue tropism.[2–5] Furthermore, other studies have demonstrated that the extreme rigidity of bone helps promote stem cell differentiation[6] and increases osteoblast differentiation and mineralization,[7] suggesting that a 3D bone mimicking microenvironment is not only critical for studying tumor behavior in bone, but also for studying the contribution of other cells present in the bone and bone marrow (BM). In **Table 1**, different types of tissue-engineered bone biomaterials are summarized with a list of their compressive strength, as this is a key parameter useful for comparing 3D tissue-engineered bone. (For a review on methods for analyzing mechanical properties of 3D tissue engineering materials, please see ref. 8).

Correspondence: Dr MR Reagan, Maine Medical Center Research Institute, 81 Research Drive, Scarborough, ME 04074, USA.
E-mail: Mreagan@mmc.org
[7]These authors contributed equally to this work.

Received 22 April 2016; accepted 6 September 2016; published online 19 October 2016

Table 1 Tissue-engineered bone used in cancer-and-bone *in vitro* modeling

Material	*Compressive modulus (dependent on strain values)*	*References*
Cortical bone	17–20 × 10^3 MPa	43
Cancellous (trabecular) bone	50–100 MPa	43
Decellularized ECM from cultured cells	NA	11,13
Decellularized bone (with tumor cell lines or cell spheroids)	125–145 MPa	9,10,44–46
Cell sheets in bioreactors on cellulose membranes	NA	47
Cell sheets over medical-grade polycaprolcatone-tricalcium phosphate scaffolds	Unknown	48
Hyaluronic acid-based hydrogels	9.3–20 kPa	16
Silk fibroin scaffolds	Varies, ~13 MPa[22] before cell-based mineralization	18,20,22, 49–52
HA (with or without with collagen I peptides)	Unreported, or ~5.5 kPa: HA + collagen ~3.24 kPa: collagen	14,15,32,53,54
Chitosan hydrogel scaffolds (with or without HA or collagen)	~5 kPa	55,56
Fibronectin/collagen I/matrigel	~2 kPa	57,58
Aqueous-derived silk scaffolds	3.33 MPa	25
HFIP-derived silk	450–1000 kPa	59
Patient tumor explants/BM supernatant of MM patients	Unknown	60,61
Gellan and xanthan polymers (reinforced with bioglass nanoparticles)	20.36 ± 1.08 MPa	7
PLG non-mineralized	~0.5 MPa	32
PLG mineralized with HA	~1.1 MPa	
63 s bioglass reinforced with 10% HA whiskers	23.69 MPa	34
63 s bioglass reinforced with 10% HA particles	19.21 MPa	
63 s bioglass scaffolds alone	~14 MPa	
β-tricalcium phosphate nanoparticles incorporated into poly(L-lactic acid)	0.2–1 MPa	35

Abbreviations: BM, bone marrow; ECM, extracellular matrix; HA, hydroxyapatite; HFIP, hexafluoroisopropanol; MM, multiple myeloma; NA, not applicable; PLG, poly(lactide-co-glycolide.

In this review, we will provide an overview of techniques currently available to study tumor interactions with bone in utilizing 3D models.

3D Models using Naturally Derived Materials

Decellularized Bone and Matrix. Decellularized bone modeling involves decellularizing native bone tissue via chemical, enzymatic, physical or combination treatments[9,10] and has recently been explored for developing *in vitro* cancer-and-bone models.[11] These models circumvent immunogenicity caused by xenografts, mimic bone structure and microarchitecture, and offer cells a tissue-appropriate template. A recent tissue-engineered model of Ewing's sarcoma describes the differential gene expression of tumor cells in 3D which results in strong upregulation of cancer-related genes, expression of hypoxic and glycolytic tumor phenotypes, and angiogenic and vasculogenic mimicry.[12] Similarly, BM and adipose-derived (AD) stromal cells have been used to generate BM-extracellular matrix (ECM) and AD-ECM, which is subsequently decellularized and seeded with specific cells of interest.[13] Although both ECMs supported proliferation of cancer cell lines (HeLa, MCF-7 and MDA-MB-231), and mesenchymal stromal cells (MSCs), they showed differences in architecture (that is, fiber orientation, surface roughness) and physical properties (storage modulus and surface energy).[13] It is debatable whether culturing on ECM is truly a 3D culture, as the tumor cells still grow in a relatively flat plane.

Hyaluronic Acid Hydrogels. Another natural 3D bone model uses hyaluronic acid-based hydrogels seeded with renal cell carcinoma cells, which form spheroids in hydrogels, proliferate more slowly, and more accurately mimic *in vivo* gene expression and cell phenotype than when grown in 2D.[14] A similar system uses prostate cancer osteoblast co-cultures in a hydrogel composed of thiolated hyaluronic acid and acrylated functionalized peptides with GRGDS integrin-binding sites and MMP-cleavable sites.[15] These models have allowed for visualization of osteoblasts (MC3T3-E1 cells) wrapping around tumoroids in co-culture.[15] However, hyaluronic acid hydrogel compressive moduli are around 9.3 kPa, or up to 22.6 kPa when crosslinked with genipin.[16] These values do not accurately mimic bone material properties and may cause tumor cell behavior that is not reflective of the native bone micro-environment. Many other material composite hydrogels of hyaluronic acid with gelatin, agarose, alginate and polyethylene glycol-g-chitosan have also been developed and described; these all remain below the 25 kPa compressive modulus range.[17]

Silk Protein. Silk fibroin is a highly versatile, biocompatible and biodegradable natural biopolymer. Highly porous (~50–500 μm pore size), cell-supporting silk scaffolds provide a 3D micro-environment for cell attachment, growth and co-culture for tumor cells.[18,19] Successful cancer-and-bone models have been demonstrated with MM cells that typically are not able to survive culture in 2D *in vitro*, but can be cultured for 2 weeks on *Bombyx mori* silk fibroin scaffolds.[18] Breast and prostate cancer cells also survive culture for up to 30 days on *Antheraea mylitta* silk scaffolds.[12,18–21]

Silk scaffolds can be either hexafluoroisopropanol (HFIP)-derived (85–1000 kPa alone to 10.64 MPa when reinforced with silk fibers)[22] or aqueous-derived (50 kPa–3.33 MPa), depending on the formulation process.[23,24] Aqueous scaffolds may better promote MSC adhesion owing to their rougher surface texture, higher modulus and more microporous topography.[24,25] Aqueous-based scaffolds also appear to

support greater bone formation *in vitro* and degrade faster *in vivo* than HFIP-derived scaffolds.[26] In the following protocols, we discuss processes for making silk scaffolds, and methods for utilizing silk scaffolds for 3D *in vitro* cancer-and-bone models.

Composites and Other Materials. Although not specifically used for bone/cancer models, many other natural materials could also be used for this application. For example, a mechanically stiff, zinc crosslinked nanocomposite scaffold with osteoinductive properties was recently described using natural, biodegradable gellan and xanthan polymers reinforced with 20–120 nm-sized bioglass nanoparticles.[7] Their compressive strength and modulus, 1.91 ± 0.31 MPa and 20.36 ± 1.08 MPa, respectively, were comparable to the trabecular bone and very high compared with nanocomposite scaffolds reported in earlier studies.[7] Porous S-sulfo keratin sponge scaffolds have also been fabricated, but their compressive strengths are unknown.[27]

3D Models using Synthetic Materials

The bone is a dichotomous tissue with a spongy marrow interior and a strong, rigid exterior. The rigid bone matrix can be mimicked by a range of synthetic materials including bioactive glass, calcium phosphates and polymer/ceramic composites, which offer robust control over structural and mechanical properties.

PURs. Polyurethanes (PURs), which are synthesized from the reaction of isocyanates (hard segment) with hydroxyls (soft segment), have been extensively used as bone and vascular grafts, and in medical devices. They are tough, durable and non-cytotoxic with tunable mechanical properties and degradation rates. PURs can be electrospun, solvent-cast or molded into defined architectures.[28] PUR scaffolds have been used to study osteogenic differentiation,[29] wound healing[30] and regeneration in the context of the bone.[31]

Although 3D printing or additive manufacturing (AM) approaches, such as Fused Deposition Modeling (FDM), enable precise control over topological properties, the limited number of materials that can be processed by AM techniques precludes precise control over mechanical properties. Below we provide methods for fabricating 3D scaffolds with substrate moduli ranging from that of collagen to trabecular bone (10–300 MPa), and pore sizes in the range that support tumor proliferation and modulate gene expression associated with metastatic disease ($>300\,\mu m$) using a t-FDM process.[29]

Poly(lactide-co-glycolide). Other synthetic materials for cancer-and-bone models include porous mineralized scaffolds composed of poly(lactide-co-glycolide) and hydroxyapatite (HA).[32] These are fabricated by a modified gas-forming/particulate-leaching method[33] and have a compressive modulus of 1.1 MPa. HA, the primary constituent of inorganic matter in the bone, is noted for its role in providing bone with exceptional tissue stiffness and serving as a reservoir of ions (that is, Ca^{2+} and PO_4^{3-}). It also represents a bioactive material that modulates the behavior of both normal and tumor cells independent of changes in material properties.[32]

Bioglass. Bioglass known as 63 s glass (63% SiO_2, 28% CaO and 9% P_2O_5 in molar percentages) has been used as a starting material for bone-cancer *in vitro* scaffold models.[34] It has been reinforced with HA nanowhiskers (500 nm length and 50 nm aspect ratio) or nanoparticles (100 nm diameter)[34] that significantly increase compressive strength and fracture toughness when compared with pure 63 s glass scaffolds. Bioglass composite scaffolds successfully cultured MG-63 osteosarcoma cells and exhibited good apatite-forming ability and cellular affinity.[34]

PLLA/β-TCP. Nanocomposite scaffolds have also been made using β-tricalcium phosphate (β-TCP) nanoparticles incorporated into poly(L-lactic acid) (PLLA) using a thermally induced phase-separation method.[35] These scaffolds with interconnected micropores utilize the good osteoconductive and osteoinductive properties of β-TCP and the biogradation abilities of PLLA.[35] MG-63 osteosarcoma cells also proliferated well on these scaffolds.[35]

Fabrication methods and protocol details

Several aspects must be considered and individualized for each study when choosing a 3D model. As described above, these parameters include matrix rigidity, chemistry, pore size and availability of tools. Here, we describe two protocols to fabricate 3D models using 'natural' and 'synthetic' materials. Silk scaffolds are excellent models to use to investigate long term (14–30 days) co-culture interactions between the bone microenvironment cells and tumor cells (for example, MM, prostate and breast cancer cells). They are highly porous, biocompatible and biodegradable. 3D-printed PUR-templated fusion deposition (see the section 't-FDM Scaffold Fabrication and Seeding for Tissue-Engineered Bone' below) are outstanding models for studying structural properties of the bone (microarchitecture, pore size, rigidity, shear stress and fluid flow) and its impact on metastatic gene expression and morphology of tumor cells (mono- and co-cultures) for both short- and long-term cultures. Both silk and printed PUR template fusion deposition scaffolds are mechanically tunable, biocompatible, and have a controllable and well-defined microarchitecture (pore sizes and scaffold shape).

Silk Scaffold Fabrication and Seeding for Tissue-Engineered Bone.
Aqueous- and HFIP-derived silk scaffolds. Silk fibroin scaffolds are fabricated using silkworm (*Bombyx mori*) cocoons (**Figures 1a–h**). In all, 5 g of silkworm cocoons are cut into small pieces, placed into 2 l of boiling 0.02 M Na_2CO_3, and boiled for 30 min. The supernatant containing silk sericin is discarded, and silk fibroin is retained and rinsed in fresh de-ionized water for 20 min 3 times. The silk is wrung out and laid to dry. In a beaker, a 9.3 M solution of LiBr is added to dried silk (20% weight silk/volume LiBr), covered and allowed to dissolve at 60 °C for 4 h. Dialysis cassettes (3500 MW cutoff) are filled with 12 ml of silk LiBr solution, which is dialyzed against 1 l de-ionized water for 3 days. The silk solution is then centrifuged for 20 min (9000 r.p.m., 5–10 °C) twice to remove debris and concentration is determined (wt/wt% or wt/vol%) by weighing a 1 ml sample 'of the solution before and after drying for 12 h at 60 °C. Silk solutions of 6–8% work well for constructing scaffolds of 500–600 μm pore sizes.

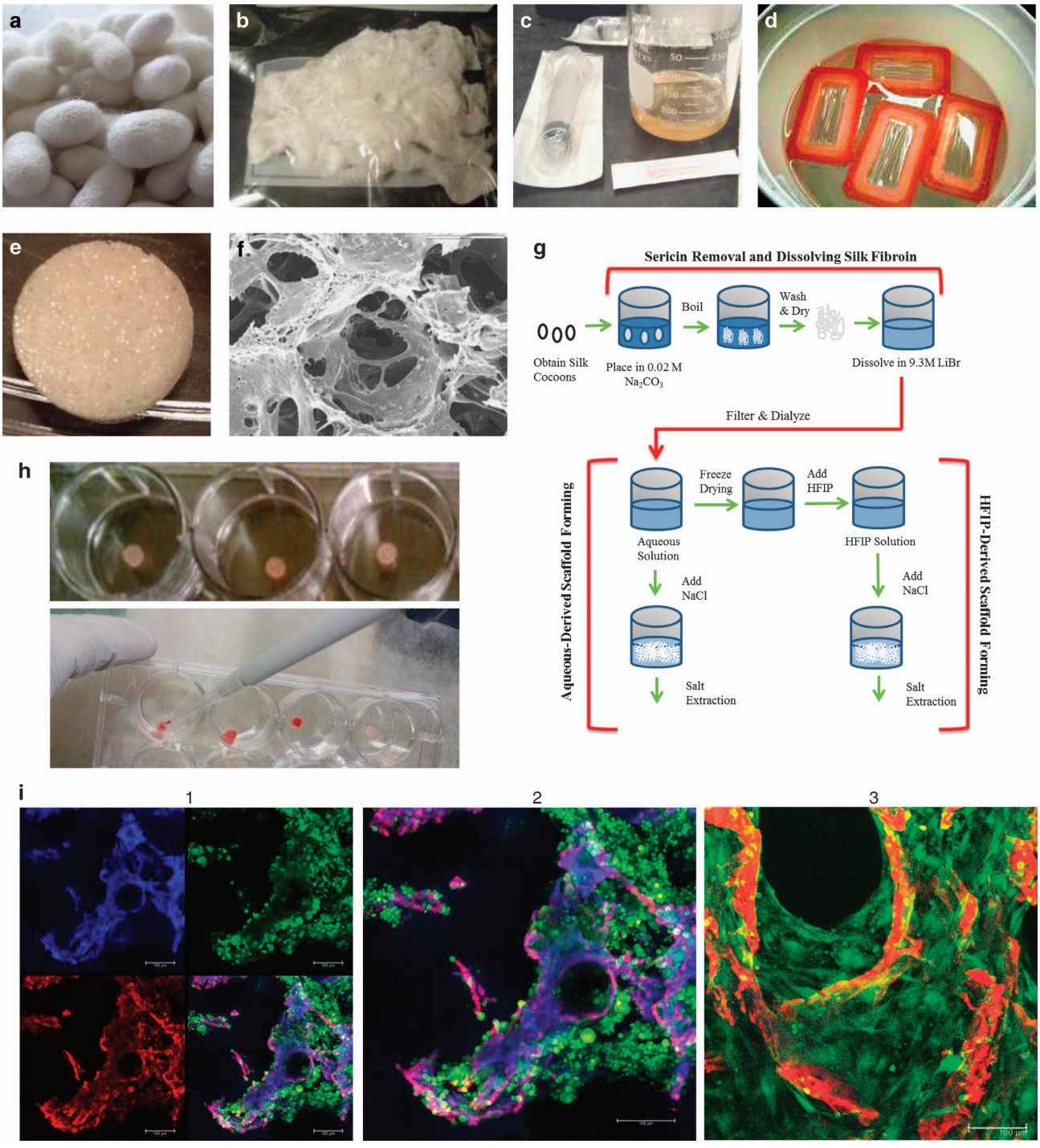

Figure 1 Generation, seeding and analysis of silk scaffolds for tissue-engineered bone-cancer models. (**a**) Silk worms (*Bombyx mori*) are grown on mulberry leaves and produce cocoons as they begin to undergo metamorphosis into silk moths. (**b**) Cleaned cocoons are boiled to separate silk sericin from silk fibroin and air dried to produce fibroin with a cottony texture. (**c**) Dried silk fibroin is then dissolved in LiBr to produce a highly concentrated silk solution. (**d**) This solution is then dialyzed with dialysis cassettes to remove LiBr ions and purify the silk solution. Silk solution can then be freeze-dried and re-dissolved by HFIP, or used directly to make silk scaffolds. (**e**) Silk solution is poured into molds and NaCl crystals are added slowly over the silk solution to crosslink silk protein to create a porous scaffold. After 3 days, salt is washed from the scaffolds and scaffolds are cut to size. (**f**) Silk scaffolds can be imaged with a scanning electron microscope (SEM) for high-resolution imaging. (**g**) Schematic of silk scaffolds making procedures. (**h**) Scaffolds are soaked in well plates (top) with culture media to prepare for seeding, and then cells are seeded with a pipette (bottom). (**i**) Whole flushed BM cells from C3H mice were seeded onto silk scaffolds and imaged with live/dead confocal imaging 3 days after seeding. (1) Silk autofluorescence is seen in the blue channel, dead cells (ethidium homodimer-1) and autofluorescence of silk is seen in the red channel, and live cells (calcein) are seen in the green channel. (2) Magnification of the overlay from shows scaffold in purple/pink, live cells in green, and a few dead cells, indicated in red. (3) Live-dead (calcein-green/ethidium homodimer-1/red) staining confocal imaging of mouse MSCs (green) first expanded *in vitro* on tissue culture plastic (2D), and then seeded at passage 2 on silk scaffolds (red) and cultured for 9 days in mMSC expansion media. Cells can be seen growing off the scaffolds and into the pores throughout the scaffolds.

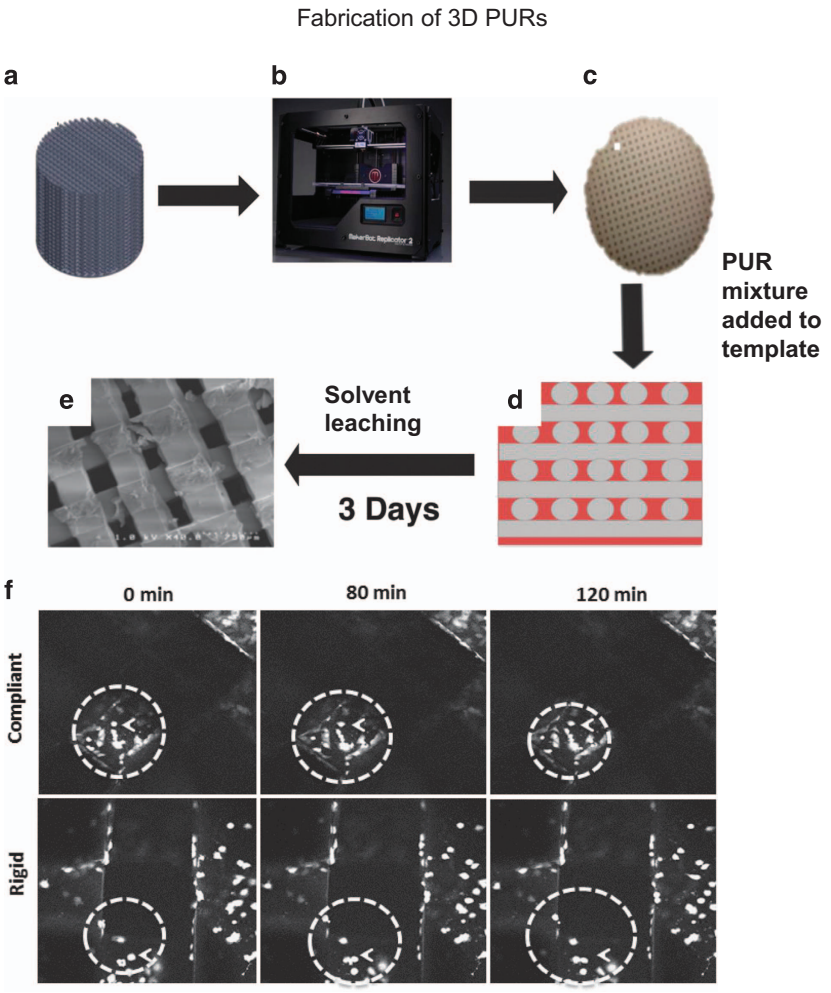

Figure 2 Fabrication schematic and analysis for t-FDM scaffolds. (**a**) Scaffold molds (inverse scaffold template) were designed in SolidWorks software with tunable pore size and physical microarchitecture as shown by representative image (**b**) PLA templates were printed using a MakerBot Replicator 2 FDM printer. (**c**) Liquid PUR is poured into the PLA templates (representative image of the scaffold mold) and this template-PUR mixture is cured overnight at 60 °C to set. (**d**) Scaffold molds are washed and the PLA is leached out using an acetone-dichloromethane-acetone solution mixture. (**e**) Representative scanning electron microscopy (SEM) image of the rigid scaffold. (**f**) GFP $^{+}$ MDA-MB-231 cells were seeded on fibronectin-coated PUR scaffolds. Scaffolds shown here mimic collagen (compliant) and trabecular bone (rigid) stiffness indices. Seeded scaffolds are incubated for 24 h, serum-starved for 6 h and placed on glass-bottom MatTek dishes to image. The cell motility of the GFP $^{+}$ MDA-MB-231 cells was observed using live confocal imaging. Representative gray-scaled confocal imaging demonstrates tumor cells (denoted in bright white, highlighted by white dotted line and white arrow following a single cell) migrating over 3D scaffold surface.

Aqueous-Derived Silk Fibroin Scaffold Preparation In all, 4 g of NaCl particles sifted through a metal mesh to obtain desired pore size (500–600 μm diameter) are slowly added to 2 ml silk fibroin aqueous solution in plastic containers. Containers are covered, sealed airtight and left at room temperature (RT) for 24 h prior to immersion in de-ionized water for 2 days to extract NaCl.

HFIP-Derived Silk Fibroin Scaffold Preparation To lyophilize silk, silk fibroin aqueous solution is pour into a 50 ml conical tube, covered with a Kimwipe secured with a rubber band and frozen at − 80 °C overnight or until fully dried. Lyophilized silk is then dissolved with HFIP to produce a 17 wt% HFIP-derived silk solution in a chemical hood. HFIP silk solution (2 ml) is poured over 4 g of NaCl particles (500–600 μm diameter) in small plastic containers, which are capped quickly and left overnight at RT. Containers are opened to allow HFIP to evaporate from scaffolds for 3 days then submerged in a 90% methanol solution for 30 min to 3 days to induce β-sheet structure formation. Finally, samples are removed and immersed in water for 3 days to remove NaCl particles to produce silk scaffolds, which are removed from containers and cut to shape.

Tissue-Engineered Bone from BM-derived MSCs. Once scaffolds are formed, they are cut to desired dimensions using a biopsy punch or razor blade to ∼4 mm diameter × 4 mm height for *in vitro* applications. To sterilize the scaffolds (if dry), scaffolds are wrapped in aluminum foil and placed into autoclavable packets and, if wet, put into a small glass, water-filled jar and autoclaved. Sterile scaffolds are soaked in media for 24 h and then cells of interest are seeded directly onto scaffolds (**Figure 1h**). For example, human MSCs (hMSCs) should be seeded at ∼17 000 cells per mm^3 in 20–40 μl media. Whenever possible, cells that stably express a fluorescent protein, such as GFP or RFP (green or red fluorescent protein) should be used. Cell type and concentrations can be modified. Scaffolds seeded with cells are incubated (37 °C, 5% CO_2) for ∼1 h to

allow cells to adhere to scaffold and then fresh media is added to cover the scaffolds. At day 5, or once scaffolds appear covered by hMSCs, osteogenic medium is added to scaffolds and cells are differentiated for as long as desired to create TE-bone (tissue-engineered bone). If tumor cells are cultured with TE-bone during or after the process of differentiation, dexamethasone should not be used in media and an alternative acceptable medium for both cell types should be determined. Medium is changed every 3 days, or as often as needed. Mineralization can be quantified with μCT or histology. For hMSCs, 1 week of proliferation and 3–4 weeks of osteogenic differentiation produces mineralized, osteoblast-containing scaffolds, depending on the cell donor.

t-FDM Scaffold Fabrication and Seeding for Tissue-Engineered Bone. Reagents. HDIt, Stannous octoate (Sigma-Aldrich, St Louis, MO, USA), glycerol (Sigma-Aldrich), poly(ε-caprolactone) triol (300 Da) (Sigma-Aldrich), ε-caprolactone (Sigma-Aldrich), glycolide (Polysciences), Fibronectin (Life Technologies, Carlsbad, CA, USA).

Materials and Methods. Glycerol is dried at 10 mm Hg overnight at 80 °C and ε-caprolactone is dried over anhydrous magnesium sulfate prior to use (~15 min). Poly(ε-caprolactone-*co*-glycolide) triol ($M_n = 3000\ g\ mol^{-1}$) is synthesized using the glycerol starter, ε-caprolactone, D,L lactide, glycolide and catalyst—stannous octoate mixed in a 100-ml reaction flask with mechanical stirring under argon for 36 h at 140 °C. The polyol then is dried under vacuum at 80 °C for 14 h. PUR scaffolds are synthesized by mixing poly(ε-caprolactone-*co*-glycolide) triol ($M_n = 300$ (add 1.98 g) or $3000\ g\ mol^{-1}$ (add 3.15 g)), hexamethylene diisocyanate trimer (HDIt (Bayer MaterialScience, Pittsburgh, PA, USA), (add 4 g (for $M_n = 300$) or 1.5 g (for $M_n = 3000$), respectively)) and stannous octoate (catalyst, (add 1.2 mg)) in a cup for 30 s with a Hauschild SpeedMixer DAC 150 FVZ-K vortex mixer (FlackTek, Landrum, SC, USA). This solution is then poured into the PLA templates as described below.

Fabrication of 3D scaffolds by templated-fused deposition modeling. Polylactic acid (PLA) template molds can be designed with varying internal microarchitecture, shape and size. For this example, we designed scaffold mold templates (14 mm diameter) with a defined 100% connected porous architecture using SolidWorks software (Waltham, MA, USA) and printed using a MakerBot Replicator 2 FDM printer (Brooklyn, NY, USA) (**Figure 2**). The PUR liquid is poured into the PLA templates to completely cover them (~500 mg) and cured at 60 °C overnight. The PLA template is then immersed in acetone (~2 h), leached with dichloromethane (use 2 × volume of the scaffolds or enough to immerse all the scaffolds), washed with acetone and then dichloromethane to yield scaffolds with interconnected pores having a channel diameter of 423 ± 34 or 557 ± 44 μm for nominal 300 or 500 μm templates, respectively[29]
(**Figures 2a–d**). Scaffolds are sterilized under ultraviolet light for 15 min in 70% ethanol, rinsed with phosphate-buffered saline (three times) and then placed in a solution of $4\ \mu g\ ml^{-1}$ fibronectin overnight at 4 °C. The substrate modulus (E_s) of the scaffolds is controlled by the M_w of the polyester triol (compliant, $3000\ g\ mol^{-1}$; rigid, $300\ g\ mol^{-1}$) to attain values representative of collagen (5 MPa, compliant), trabecular bone (266 MPa, rigid) or cortical bone (871–11 500 MPa).[36,37]

Cell viability, proliferation and metabolic activity. Trypan Blue cell viability, live/dead staining (calcein/propidium homodimer) or MTS assays (CellTiter 96 Aqueous Non-Radioactive Cell Proliferation Assay, Promega, Madison, WI, USA) can be performed as per the manufacturers' protocols.

Bioreactor experiments. Scaffolds are cultured in a flow perfusion bioreactor (3D Biotek, North Brunswick Township, NJ, USA). During bioreactor culture, scaffolds can be placed in individual autoclavable polycarbonate chambers and seeded with 0.25 to 1×10^6 GFP^+ MDA-MB-231 cells per scaffold. These scaffolds then can be studied simultaneously using a steady flow regime for 48 h at $9.35\ \mu l\ s^{-1}$ (an optimal flow rate for MDA-MB-231 cells). This flow rate equates to osteogenic inductive fluid shear stress, τ (~0.0176 Pa).[38,39] Culture medium (either standard or supplemented with study drugs) is perfused through the open porous structure of scaffolds using a pulsatile pump feeding into a media reservoir chamber. Within each chamber there is a 1.5 mm distance separating each scaffold. The whole system, including the pump, is placed in a 5% CO_2, 37 °C incubator. After culture scaffolds are harvested for gene or protein expression.

Analysis Protocols. Both silk scaffolds and PUR 3D-printed scaffolds can be imaged or analyzed with confocal microscopy (**Figures 1i and 2f**), flow cytometry to measure changes in cell populations, immunohistochemistry, scanning electron microscopy and bioluminescence imaging. These procedures require little modification from typical protocols, and thus will not be discussed here.

Cell isolation from scaffolds for downstream analysis. Cells are trypsinized from scaffolds, and fluorescence is used to quantify and separate cells into different populations when needed. Scaffolds are flash frozen in liquid nitrogen and then crushed using a mortar and pestle to extract cells for mRNA or microRNA expression from total RNA using Qiagen miRNeasy Kits (Qiagen, Hilden, Germany).

Immunohistochemistry. After desired co-culture period, silk scaffolds can be fixed in 4% paraformaldehyde overnight, paraffin embedded and stained for markers such as alizarin red (mineralization), hematoxylin and eosin or immunohistochemisty for proteins of interest, such as CD138 in myeloma. For histological assessment of *in vivo* 3D-printed scaffolds, animals are killed, and these scaffolds can be excised and processed using paraffin embedding. When sectioning scaffolds, keep paraffin block cold by placing on ice. Ensure the microtome blade is sharp and kept clean as not to snag and tear the section. After placing the section on slide make certain the section is placed firmly on the slide. Leave the slides to dry overnight at room temperature or for ~8 h on a slide warmer.

Cell sources

hMSCs, mouse MSCs or osteoblast lineage cell lines are seeded onto scaffolds and tumor cells are added when desired.

Alternatively, whole BM can be directly seeded onto scaffolds (**Figure 1**) using previously published methods.[18,40]

Human BM cell source

Human stromal cells are isolated fresh from BM as previously described.[18] Briefly, 25 ml BM is spun at 1200 r.p.m. for 5 min at 4 °C and then gently removed from centrifuge. BM adipose is congealed at the top of this liquid, which should be aspirated using low suction without disturbing the marrow. BM is transferred to a larger flask, mixed with 224 ml hMSC expansion media, and evenly distributed to 14 deep T-185 flasks (20 ml per flask). Flasks are rocked daily. Medium (20 ml) is added to flasks every 3 days for 9 days, removing nothing. At day 10, adherent colonies are analyzed under a microscope for confluency. Alternatively, there are many commercial sources of mouse and human BM and purified MSCs.

Conclusions

In this article, we described the methods necessary for developing and validating a variety of tissue engineering models for cancer-and-bone interactions. There is an urgent need to develop and validate reliable *in vitro* models to reproduce specific tissue-like structures and mimic functions and responses of tissues in a physiological manner. These models must be physiologically relevant 3D platforms to bridge the gap between 2D and *in vivo* animal model-based cancer research. Indeed, over the past two decades, accumulating evidence about various organs and disease models has demonstrated that the biochemically and spatially defined network of ECM, cellular components, and interactions that dictate cell differentiation, proliferation and function *in vivo* are lost in simplified 2D conditions, but captured with 3D models.[41] For example, the substrate modulus of the tissue surrounding a tumor significantly affects tumor cell behavior, gene expression, phenotype and invasion potential.[37,42] 3D models can thus accelerate the translation from pre-clinical to clinical trials by more accurately predicting disease course, responsive subpopulations or treatment responses, especially when using humanized, engineered bone rather than mouse bone. The protocols and methods summarized here are some of the best available tools for modeling tumors within the BM. These models have the potential to support personalized medicine through patient specific model development. Finally, the models described here enable screening of new therapeutics in a dynamic *in vitro* system prior to pre-clinical testing to allow for investigation of effects on tumor cells and microenvironmental cells.

Conflict of Interest

The authors declare no conflict of interest.

Acknowledgements

This work is supported by AR066120, R24 DK092759, P41 EB002520, P30 GM106391, P30 GM103392, Schlumberger Faculty for the Future pre-doctoral program (UCD), 1I01BX001957 (JAS) and R01CA163499 (SAG/JAS). We thank Dr Michael Erard, Scientific Editor and Writing Consultant at MMCRI, for manuscript editing and Dr Amanda Murphy, Western Washington University, for her beautiful photographs of silk cocoons (shown in **Figure 1a**).

References

1. Coleman RE. Skeletal complications of malignancy. *Cancer* 1997; **80**: 1588–1594.
2. Kostic A, Lynch CD, Sheetz MP. Differential matrix rigidity response in breast cancer cell lines correlates with the tissue tropism. *PLoS ONE* 2009; **4**: e6361.
3. Butcher DT, Alliston T, Weaver VM. A tense situation: forcing tumour progression. *Nat Rev Cancer* 2009; **9**: 108–122.
4. Engler AJ, Sen S, Sweeney HL, Discher DE. Matrix elasticity directs stem cell lineage specification. *Cell* 2006; **126**: 677–689.
5. Paszek MJ, Zahir N, Johnson KR, Lakins JN, Rozenberg GI, Gefen A *et al.* Tensional homeostasis and the malignant phenotype. *Cancer Cell* 2005; **8**: 241–254.
6. Guo R, Ward CL, Davidson JM, Duvall CL, Wenke JC, Guelcher SA. A transient cell-shielding method for viable MSC delivery within hydrophobic scaffolds polymerized in situ. *Biomaterials* 2015; **54**: 21–33.
7. Sehgal RR, Carvalho E, Banerjee R. Mechanically stiff, zinc cross-linked nanocomposite scaffolds with improved osteostimulation and antibacterial properties. *ACS Appl Mater Interfaces* 2016; **8**: 13735–13747.
8. Vazquez OR, Avila IO, Díaz JCS, Hernandez E. An overview of mechanical tests for polymeric biomaterial scaffolds used in tissue engineering. *J Res Updat Polym Sci* 2016; **4**: 168–178.
9. Gilbert TTW. Strategies for tissue and organ decellularization. *J Cell Biochem* 2012; **113**: 2217–2222.
10. Anisimova NY, Kiselevsky MV, Sukhorukova IV, Shvindina NV, Shtansky DV. Fabrication method, structure, mechanical, and biological properties of decellularized extracellular matrix for replacement of wide bone tissue defects. *J Mech Behav Biomed Mater* 2015; **49**: 255–268.
11. Reichert JC, Quent VMC, Burke LJ, Stansfield SH, Clements JA, Hutmacher DW. Mineralized human primary osteoblast matrices as a model system to analyse interactions of prostate cancer cells with the bone microenvironment. *Biomaterials* 2010; **31**: 7928–7936.
12. Villasante A, Vunjak-Novakovic G. Tissue-engineered models of human tumors for cancer research. *Expert Opin Drug Discov* 2015; **10**: 257–268.
13. Marinkovic M, Block TJ, Rakian R, Li Q, Wang E, Reilly MA *et al.* One size does not fit all: developing a cell-specific niche for *in vitro* study of cell behavior. *Matrix Biol* 2016; **52–54**: 426–441.
14. Pan T, Fong ELS, Martinez M, Harrington DA, Lin S-H, Farach-Carson MC *et al.* Three-dimensional (3D) culture of bone-derived human 786-O renal cell carcinoma retains relevant clinical characteristics of bone metastases. *Cancer Lett* 2015; **365**: 89–95.
15. Fong ELS, Wan X, Yang J, Morgado M, Mikos AG, Harrington DA *et al.* A 3D in vitro model of patient-derived prostate cancer xenograft for controlled interrogation of in vivo tumor-stromal interactions. *Biomaterials* 2015; **77**: 164–172.
16. Tan H, Li H, Rubin JP, Marra KG. Controlled gelation and degradation rates of injectable hyaluronic acid-based hydrogels through a double crosslinking strategy. *J Tissue Eng Regen Med* 2011; **5**: 790–797.
17. Cloyd JM, Malhotra NR, Weng L, Chen W, Mauck RL, Elliott DM. Material properties in unconfined compression of human nucleus pulposus, injectable hyaluronic acid-based hydrogels and tissue engineering scaffolds. *Eur Spine J* 2007; **16**: 1892–1898.
18. Reagan MR, Mishima Y, Glavey SV, Zhang Y, Manier S, Lu ZN *et al.* Investigating osteogenic differentiation in multiple myeloma using a novel 3D bone marrow niche model. *Blood* 2014; **124**: 3250–3259.
19. Talukdar S, Mandal M, Hutmacher DW, Russell PJ, Soekmadji C, Kundu SC. Engineered silk fibroin protein 3D matrices for *in vitro* tumor model. *Biomaterials* 2011; **32**: 2149–2159.
20. Kwon H, Kim HJ, Rice WL, Subramanian B, Park S-H, Georgakoudi I *et al.* Development of an *in vitro* model to study the impact of BMP-2 on metastasis to bone. *J Tissue Eng Regen Med* 2010; **4**: 590–599.
21. Bhardwaj N, Nguyen QT, Chen AC, Kaplan DL, Sah RL, Kundu SC. Potential of 3-D tissue constructs engineered from bovine chondrocytes/silk fibroin-chitosan for in vitro cartilage tissue engineering. *Biomaterials* 2011; **32**: 5773.
22. Mandal BB, Grinberg A, Gil ES, Panilaitis B, Kaplan DL. High-strength silk protein scaffolds for bone repair. *Proc Natl Acad Sci USA* 2012; **109**: 7699–7704.
23. Wray LS, Rnjak-Kovacina J, Mandal BB, Schmidt DF, Gil ES, Kaplan DL. A silk-based scaffold platform with tunable architecture for engineering critically-sized tissue constructs. *Biomaterials* 2012; **33**: 9214–9224.
24. Correia C, Bhumiratana S, Yan L-P, Oliveira AL, Gimble JM, Rockwood D *et al.* Development of silk-based scaffolds for tissue engineering of bone from human adipose-derived stem cells. *Acta Biomater* 2012; **8**: 2483–2492.
25. Kim U-J, Park J, Kim HJ, Wada M, Kaplan DL. Three-dimensional aqueous-derived biomaterial scaffolds from silk fibroin. *Biomaterials* 2005; **26**: 2775–2785.
26. Kim HJ, Kim U-J, Vunjak-Novakovic G, Min B-H, Kaplan DL. Influence of macroporous protein scaffolds on bone tissue engineering from bone marrow stem cells. *Biomaterials* 2005; **26**: 4442–4452.
27. Katoh K, Tanabe T, Yamauchi K. Novel approach to fabricate keratin sponge scaffolds with controlled pore size and porosity. *Biomaterials* 2004; **25**: 4255–4262.
28. Guelcher SA. Biodegradable polyurethanes: synthesis and applications in regenerative medicine. *Tissue Eng Part B Rev* 2008; **14**: 3–17.

29. Guo R, Lu S, Page JM, Merkel AR, Basu S, Sterling JA *et al.* Fabrication of 3D scaffolds with precisely controlled substrate modulus and pore size by templated-fused deposition modeling to direct osteogenic differentiation. *Adv Healthc Mater* 2015; **41826–1832.**
30. Guo R, Merkel AR, Sterling JA, Davidson JM, Guelcher SA. Substrate modulus of 3D-printed scaffolds regulates the regenerative response in subcutaneous implants through the macrophage phenotype and Wnt signaling. *Biomaterials* 2015; **73**: 85–95.
31. Talley AD, Kalpakci KN, Shimko DA, Zienkiewicz KJ, Cochran DL, Guelcher SA. Effects of recombinant human bone morphogenetic protein-2 dose and ceramic composition on new bone formation and space maintenance in a canine mandibular ridge saddle defect model. *Tissue Eng Part A* 2016; **22**: 469–479.
32. Pathi SP, Kowalczewski C, Tadipatri R, Fischbach C. A novel 3-D mineralized tumor model to study breast cancer bone metastasis. *PLoS ONE* 2010; **5**: e8849.
33. Kim S-S, Sun Park M, Jeon O, Yong Choi C, Kim B-S. Poly(lactide-co-glycolide)/hydroxyapatite composite scaffolds for bone tissue engineering. *Biomaterials* 2006; **27**: 1399–1409.
34. Shuai C, Cao Y, Gao C, Feng P, Xiao T, Peng S. Hydroxyapatite whisker reinforced 63 s glass scaffolds for bone tissue engineering. *Biomed Res Int* 2015; **2015**: 379294.
35. Lou T, Wang X, Song G, Gu Z, Yang Z. Structure and properties of PLLA/β-TCP nanocomposite scaffolds for bone tissue engineering. *J Mater Sci Mater Med* 2015; **26**: 5366.
36. Lynch ME, Fischbach C. Biomechanical forces in the skeleton and their relevance to bone metastasis: biology and engineering considerations. *Adv Drug Deliv Rev* 2014; **79–80**: 119–134.
37. Page JM, Merkel AR, Ruppender NS, Guo R, Dadwal UC, Cannonier SA *et al.* Matrix rigidity regulates the transition of tumor cells to a bone-destructive phenotype through integrin β3 and TGF-β receptor type II. *Biomaterials* 2015; **64**: 33–44.
38. McCoy RJ, O'Brien FJ. Influence of shear stress in perfusion bioreactor cultures for the development of three-dimensional bone tissue constructs: a review. *Tissue Eng Part B Rev* 2010; **16**: 587–601.
39. McCoy RJ, Jungreuthmayer C, O'Brien FJ. Influence of flow rate and scaffold pore size on cell behavior during mechanical stimulation in a flow perfusion bioreactor. *Biotechnol Bioeng* 2012; **109**: 1583–1594.
40. Roccaro AM, Sacco A, Maiso P, Azab AK, Tai Y-T, Reagan M *et al.* BM mesenchymal stromal cell-derived exosomes facilitate multiple myeloma progression. *J Clin Invest* 2013; **123**: 1542–1555.
41. Mazzoleni G, Di Lorenzo D, Steimberg N. Modelling tissues in 3D: the next future of pharmaco-toxicology and food research? *Genes Nutr* 2009; **4**: 13–22.
42. Ruppender NS, Merkel AR, Martin TJ, Mundy GR, Sterling JA, Guelcher SA. Matrix rigidity induces osteolytic gene expression of metastatic breast cancer cells. *PLoS ONE* 2010; **5**: e15451.
43. Cullinane D, Einhorn T. Biomechanics of bone. In: JPB, LGR, GA R (eds). *Principles of Bone Biology*. Academic Press: San Diego, CA, USA, 2001, pp 17–32.
44. Correia C, Grayson WL, Park M, Hutton D, Zhou B, Guo XE *et al. In vitro* model of vascularized bone: synergizing vascular development and osteogenesis. *PLoS ONE* 2011; **6**: e28352.
45. Grayson WL, Fröhlich M, Yeager K, Bhumiratana S, Chan ME, Cannizzaro C *et al.* Engineering anatomically shaped human bone grafts. *Proc Natl Acad Sci USA* 2010; **107**: 3299–3304.
46. Villasante A, Marturano-Kruik A, Vunjak-Novakovic G. Bioengineered human tumor within a bone niche. *Biomaterials* 2014; **35**: 5785–5794.
47. Mastro AM, Vogler EA. A three-dimensional osteogenic tissue model for the study of metastatic tumor cell interactions with bone. *Cancer Res* 2009; **69**: 4097–4100.
48. Sieh S, Lubik AA, Clements JA, Nelson CC, Hutmacher DW. Interactions between human osteoblasts and prostate cancer cells in a novel 3D *in vitro* model. *Organogenesis* **6**: 181–188.
49. Kim HJ, Kim U-J, Leisk GG, Bayan C, Georgakoudi I, Kaplan DL. Bone regeneration on macroporous aqueous-derived silk 3-D scaffolds. *Macromol Biosci* 2007; **7**: 643–655.
50. Kim HSHJ, Kim U-J, Kim HSHJ, Li C, Wada M, Leisk GG *et al.* Bone tissue engineering with premineralized silk scaffolds. *Bone* 2008; **42**: 1226–1234.
51. Augst A, Marolt D, Freed LE, Vepari C, Meinel L, Farley M *et al.* Effects of chondrogenic and osteogenic regulatory factors on composite constructs grown using human mesenchymal stem cells, silk scaffolds and bioreactors. *J R Soc Interface* 2008; **5**: 929–939.
52. Marolt D, Augst A, Freed LE, Vepari C, Fajardo R, Patel N *et al.* Bone and cartilage tissue constructs grown using human bone marrow stromal cells, silk scaffolds and rotating bioreactors. *Biomaterials* 2006; **27**: 6138–6149.
53. Yang XB, Bhatnagar RS, Li S. Oreffo ROC. Biomimetic collagen scaffolds for human bone cell growth and differentiation. *Tissue Eng* **10**: 1148–1159.
54. Cholas R, Kunjalukkal Padmanabhan S, Gervaso F, Udayan G, Monaco G, Sannino A *et al.* Scaffolds for bone regeneration made of hydroxyapatite microspheres in a collagen matrix. *Mater Sci Eng C* 2016; **63**: 499–505.
55. Zhu W, Wang M, Fu Y, Castro NJ, Fu SW, Zhang LG. Engineering a biomimetic three-dimensional nanostructured bone model for breast cancer bone metastasis study. *Acta Biomater* 2015; **14**: 164–174.
56. Arakawa C, Ng R, Tan S, Kim S, Wu B, Lee M. Photopolymerizable chitosan-collagen hydrogels for bone tissue engineering. *J Tissue Eng Regen Med* 2014.
57. Kirshner J, Thulien KJ, Martin LD, Debes Marun C, Reiman T, Belch AR *et al.* A unique three-dimensional model for evaluating the impact of therapy on multiple myeloma. *Blood* 2008; **112**: 2935–2945.
58. O'Leary C, Cavanagh B, Unger RE, Kirkpatrick CJ, O'Dea S, O'Brien FJ *et al.* The development of a tissue-engineered tracheobronchial epithelial model using a bilayered collagen-hyaluronate scaffold. *Biomaterials* 2016; **85**: 111–127.
59. Nazarov R, Jin H-J, Kaplan DL. Porous 3-D scaffolds from regenerated silk fibroin. *Biomacromolecules* 2004; **5**: 718–726.
60. Ferrarini M, Steimberg N, Ponzoni M, Belloni D, Berenzi A, Girlanda S *et al. Ex-vivo* dynamic 3-D culture of human tissues in the RCCS bioreactor allows the study of Multiple Myeloma biology and response to therapy. *PLoS ONE* 2013; **8**: e71613.
61. de la Puente P, Muz B, Gilson RC, Azab F, Luderer M, King J *et al.* 3D tissue-engineered bone marrow as a novel model to study pathophysiology and drug resistance in multiple myeloma. *Biomaterials* 2015; **73**: 70–84.